JOURNAL OF Materials CHEMISTRY

Low temperature synthesis of nanocrystalline $Y_3Al_5O_{12}$ (YAG) and Ce-doped $Y_3Al_5O_{12}$ *via* different sol–gel methods

Michael Veith,[a] Sanjay Mathur,[a] Aivaras Kareiva,[b] Mohammad Jilavi,[c] Michael Zimmer[a] and Volker Huch[a]

[a]*Institute of Inorganic Chemistry, University of Saarland, D-66041 Saarbruecken, Germany. E-mail: veith@rz.uni-sb.de*
[b]*Department of General and Inorganic Chemistry, Vilnius University, LT-2006 Vilnius, Lithuania*
[c]*Institute of New Materials, GmbH, D-66123 Saarbruecken, Germany*

Received 7th May 1999, Accepted 3rd September 1999

Nanocrystalline yttrium aluminium garnet (YAG, $Y_3Al_5O_{12}$) and Ce-doped YAG ceramics were synthesized by two 'soft chemistry' sol–gel processes using (i) mixtures of inorganic salts or oxides and (ii) mixtures of alkoxides of the respective elements. In the first approach the metal ions, generated by dissolving metal oxides or nitrates in acetic acid and/or water, were complexed by ethylene glycol to obtain the precursors for pure and doped YAG samples. In the alkoxide route monolithic gels were obtained by hydrolysis and condensation of a compositional mixture of Al, Y and Ce alkoxides in a Pr^iOH solution. The molecular level mixing and the tendency of partially hydrolysed alkoxide species to form extended networks of cross-linked metal centers facilitates the structure evolution thereby lowering the crystallization temperature, in the latter case. The X-ray diffraction (XRD) patterns of the ceramic sintered at 700 °C were identical with the stoichiometric YAG composition which is the lowest temperature reported for the synthesis of crystalline and single phase $Y_3Al_5O_{12}$ while well developed YAG phases in the non-alkoxide synthesis were obtained only at 1000 °C. Cerium doped YAG powders ($CeO_2 + Y_3Al_5O_{12}$) were synthesized using $[NH_4]_2[Ce(NO_3)_6]$ (8 mol%) and $[Ce_3(OBu^t)_9(Bu^tOH)_2]$ (5 mol%), as dopants. A homogeneous distribution of cerium in the YAG lattice was achieved in both cases. The thermal behaviour, phase transformations, composition and microstructural features in the gels and polycrystalline samples were studied by TG/DTA, XRD, FT-IR, solid-state ^{27}Al MAS NMR spectroscopy, SEM, TEM, energy dispersive X-ray analysis and high resolution electron microscopy studies. The quality of the resulting products (homogeneity, crystallization temperature, grain size, grain size distribution, *etc.*) and economical aspects (synthetic skill, cost of precursors, *etc.*) of the two approaches are discussed.

Introduction

Ceramics based on the Y_2O_3–Al_2O_3 combination are promising materials for optical, electronic and structural applications. The composition $3Y_2O_3 : 5Al_2O_3$ commonly called yttrium aluminium garnet (YAG) adopts the cubic garnet structure and when doped with a transition metal or lanthanide element YAG is an important solid-state laser material widely used in luminescence systems and window materials for a variety of lamps.[1–7] In view of the high-temperature chemical stability and an extremely high creep resistance, YAG is a promising fiber material for the preparation of ceramic composites.[8–17] The electrical conductivity of YAG is also reported to be lower than that of any other polycrystalline oxide.[18] Owing to such wide and diverse application potential of YAG-based ceramics, new routes for the synthesis of pure and homogeneously doped yttrium aluminium garnet are highly desirable.

The solid-state synthesis of YAG ceramic from Al_2O_3 and Y_2O_3 powders usually requires extensive mechanical mixing and lengthy heat treatments above 1600 °C.[5,6,16] These processing conditions do not allow facile control over microstructure, grain size and grain size distribution in the resulting powders or shapes. Several wet-chemical techniques such as the polymerized complex route,[19] metal–organic preceramic processing,[20] coprecipitation methods[21,22] or yttrium carboxylate-alumoxane route[23] have been used to produce YAG phases. Most of these methods suffer from complex and time consuming (long refluxing times, gelation periods of several days, *etc.*) procedures and/or mismatch in the solution behaviour of the constituents. For example, simple solution mixing of the components does not guarantee a precise control of cationic stoichiometry due to the phase separation tendencies of unimetal phases. Also, the difference in the isoelectric points (different pH level) of the constituent species may result in element segregation and non-ideal stoichiometries in the obtained ceramic, *e.g.* in the synthesis of the $Y_3Al_5O_{12}$ phase, from aqueous sols of yttria and alumina, significant amounts of Y_2O_3, Al_2O_3, $YAlO_3$ and $Y_2Al_4O_9$ phases are present, even above 1650 °C.[19] The sol–gel methods based on molecular precursors have a cutting edge over the other solution routes because they allow chemical interactions (*e.g.* cross-linking of different metal centers in the case of multi-component systems) among the initial mixture of precursor species favoring the evolution of solid-state structure at the atomic level. Furthermore, the unique properties of most mixed-cation oxide ceramics depend largely on impurities or dopants [*e.g.* Ln^{3+}-doped YAG ceramics (Ln = Ce, Nd, Pr, Ho or Tb) as solid-state laser material, Nb-doped lead zirconate–lead titanate (PZT) for piezo electrics]. In the context of doped materials, the homogeneous incorporation of secondary phases in a host matrix poses a challenge to conventional powder milling methods and the fabrication of mixed oxide phases by a molecular level approach is of significant interest. However, sol–gel preparation of YAG using metal alkoxides is limited to so-called semi-alkoxide routes where generally the commercially available aluminium alkoxides have been used.[9,24–26] We

have previously shown the potential of alkoxide precursors for chemically controlled synthesis of oxides and composites by sol–gel and CVD techniques.[27–32] Also, a relatively simple aqueous sol–gel process based on the *in situ* generation of water soluble mixed-metal complexes (*e.g.* acetates, tartarates, citrates) has been employed to synthesize different pure and substituted superconducting oxides.[33–36] We evaluate here synthetic approaches to pure and Ce-doped YAG ceramics using glycolate and alkoxide intermediates which illustrate the simplicity and superior potential of the low-temperature methods.

Experimental

The synthesis of alkoxide precursors was performed using standard vacuum line and modified Schlenk techniques, taking precautions against atmospheric moisture. The hydrocarbon solvents and alcohols employed in the synthesis of alkoxide and amide precursors were dried using standard procedures and stored over molecular sieves. Yttrium and cerium amides were synthesized according to reported procedures.[37] $Al(NO_3)_3{\cdot}9H_2O$, Y_2O_3 and $[NH_4]_2[Ce(NO_3)_6]$ were of analytical grade, $[Y_3(OBu^t)_9(Bu^tOH)_2]$ and $[Ce_3(OBu^t)_9(Bu^tOH)_2]$ were obtained from respective amides by their reactions with *tert*-butyl alcohol. Aluminium *tert*-butoxide was synthesized by the reaction of Al turnings with Bu^tOH in the presence of small amounts of $HgCl_2$ (catalyst).[38]

The TGA/DTA measurements were performed on a STA 490 analyser (Netzsch, Germany). The precursors were heated (20–1200 °C) in air at a rate of 5 °C min^{-1}. The experiments were performed in quartz crucibles which also served as the reference. The calcination of raw powders was performed in a preheated laboratory tube furnace coupled with a temperature programming device. The infrared spectra were recorded as KBr pellets on a BioRad FTIR-165 spectrometer. C, H and N contents in the gels and calcined powders were obtained using a LECO CHN900 elemental analyser. The solid-state ^{27}Al NMR spectra of polycrystalline samples (*ca.* 200–250 mg) were obtained on a Bruker MSL 200S spectrometer. Powder X-ray diffraction measurements were performed at room temperature on a Siemens D-500 diffractometer operating with Cu-Kα radiation. Scanning electron microscopy was used to study the morphology of the gels before and after heat treatment. The SEM and energy dispersive X-ray (EDX) analysis were performed, in vacuum, in the specimen chamber of an EDX coupled scanning electron microscope CAM SCAN S4. The TEM images were recorded on a JEM 200 CX transmission electron microscope. High resolution electron microscopy experiments were performed on a CM-200 FEG (Philips) transmission electron microscope equipped with a field emission gun operating at 200 kV. High resolution micrographs were recorded with a slow scan CCD camera. The X-ray photoelectron spectroscopy (XPS) analyses were performed on a Surface Science Instrument SSI-M-Probe using Al-Kα radiation. The data were charge referenced to O 1s at a binding energy of 530.5 eV.

The electrical conductivities were measured on disk specimens (10 mm in diameter) of crystalline ceramics with the standard two-probe method as a function of temperature in the range 20–160 °C. The copper wire electrodes were attached to the sample pellets using a silver paste.

X-Ray crystallography

A suitable specimen of $[Y_3(OBu^t)_9(Bu^tOH)_2]$ was sealed under an inert atmosphere in a Lindemann capillary and mounted on the goniometer of a Stoe AED 2 diffractometer operating with graphite monochromated Mo-Kα X-ray radiation ($\lambda = 0.71073$ Å). Crystal data and structure refinement parameters are given in Table 1. Unit cell dimensions were determined from the least-squares refinement of $(\sin\theta/\lambda)^2$ values for 25 accurately centered reflections. The intensities were corrected for Lorentz polarisation factors, and a semi-empirical absorption correction (ψ scans) was applied. The positions of heavy atoms were determined by direct methods (SHELXS 97).[39a] The refinements were carried out using full-matrix least squares techniques (SHELXL 97).[39b]

CCDC reference number 1145/181.

See http://www.rsc.org/suppdata/jm/1999/3069/ for crystallographic files in .cif format.

Table 1 Crystal and structure refinement data for $[Y_3(OBu^t)_9(Bu^tOH)_2]$

Empirical formula	$C_{44}H_{101}O_{11}Y_3$
Formula weight	1072.98
Crystal system	Monoclinic
Space group	$P2_1/c$
a/Å	19.431(13)
b/Å	10.867(6)
c/Å	27.554(2)
β/°	99.15(6)
V/Å^3	5744(6)
Z	4
μ/mm^{-1}	3.052
T/K	293(2)
Reflections collected	7522
Independent reflections	7522
Goodness of fit on F^2	1.181
Final $R1$, $wR2$ [$I > 2\sigma(I)$]	0.0965, 0.1400
(all data)	0.2186, 0.1872

Synthesis I (glycolate method)

Yttrium oxide (0.847 g, 3.75 mmol) was dissolved in 150 ml of 0.2 mol L^{-1} CH_3CO_2H by stirring the mixture for 10 h at 55–60 °C in a beaker covered with a watch-glass. Aluminium nitrate (4.688 g, 12.5 mmol) dissolved in 50 mL of distilled water was added and the resulting mixture stirred for 2 h at the same temperature. In the case of Y–Al–Ce–O gel, an aqueous solution (50 ml) of ammonium cerium(IV) nitrate (0.206 g, 0.375 mmol) was added. 1,2-Ethanediol (25 mmol) as complexing agent was added to the above solutions. The acidic medium (pH ≈ 5) prevents flocculation of metal hydroxides in the mixtures and no adjustment of pH was necessary. After concentrating the solutions by slow evaporation at 60–70 °C with stirring, the Y–Al acetate–nitrate–glycolate solution turned into a white transparent gel while the Ce-containing solution gave a light yellow gel. The oven dried (100–120 °C) gels became light brown due to initial decomposition of nitrates. The synthesis of precursor gels for Al_2O_3 and Y_2O_3 was carried out under similar conditions. The gel powders were ground in an agate mortar and preheated for 2 h at 800 °C in air. Since the gels are very combustible slow heating (≈2 °C min^{-1}) especially between 150 and 400 °C was found to be essential. After an intermediate grinding the powders were additionally sintered at various temperatures from 800 to 1600 °C in air. The annealing time was 6 h.

Synthesis II (alkoxide method)

$[Al_2(OBu^t)_6]$ (1.40 g, 1.89 mmol) was dissolved in Pr^iOH and a 1.0–2.0 M solution of water in isopropyl alcohol added dropwise, with vigorous stirring. To this activated solution (sol), a Pr^iOH solution (30 ml) of a stoichiometric amount of $[Y_3(OBu^t)_9(Bu^tOH)_2]$ (1.22 g, 1.13 mmol) was added and the mixture stirred for 12 h to obtain a homogeneous suspension. Slow evaporation of the solvent followed by overnight aging under an inert atmosphere produced a transparent gel which was dried in vacuum at 80 °C (4 h) to obtain a white powder. The resulting material was heated in a laboratory furnace at 300 °C to burn out the organic residues and calcined at higher

temperatures (600–1200 °C) to obtain crystalline $Y_3Al_5O_{12}$. The pale yellow Ce-doped gel was synthesized analogously by using the calculated amounts of $[Al_2(OBu^t)_6]$ (1.66 g, 2.25 mmol), $[Y_3(OBu^t)_9(Bu^tOH)_2]$ (1.45 g, 1.35 mmol) and $[Ce_3(OBu^t)_9(Bu^tOH)_2]$ (0.083 g, 0.07 mmol). The pre-hydrolysis of aluminium alkoxide is a desired step for phase homogeneity. When stoichiometric mixtures of Y and Al alkoxides were simultaneously hydrolysed and processed in a similar manner to that described above the formation of metastable $YAlO_3$ was observed (till 1200 °C). Also, this approach of using a stoichiometric mixture is not applicable for Ce-doped gels and an activated aluminium alkoxide sol and a sequential (Al, Y, Ce) addition of the constituents was necessary to obtain monophasic products. The degree of hydrolysis required to obtain stable sols and to avoid precipitation was in the range 1–2.

Synthesis III (solid state reaction)

Yttrium oxide (1.141 g, 5.05 mmol) was carefully mixed with aluminium oxide (0.859 g, 8.42 mmol) in an agate mortar. The mixture was sintered for 8 h at 1000 °C in air. After an intermediate grinding the powders were pressed into pellets and additionally sintered for 16 h at 1000 °C in air with intermediate grinding steps.

Results and discussion

Chemical syntheses, in recent years, have attracted significant attention as low-temperature alternative routes to multi-component ceramic materials.[40–45] Whereas in the alkoxide based sol–gel process the gel structure itself provides the rheological properties necessary for spinning or coating, a spinning aid (*e.g.* organic polymer) is necessary for non-alkoxide preparation. However, the use of the alkoxide approach is restricted due to the rather difficult synthesis and the limited commercial availability of various metal alkoxides.[42] In this context, a potential and inexpensive alternative involves the use of metal salts and their reaction with chelating agents like ethylene glycol, acetic, tartaric or citric acid to form water soluble complexes which can be decomposed to obtain the desired ceramic materials. We report here on the synthesis of pure and Ce-doped nano-crystalline YAG ceramics from (i) glycolate and (ii) alkoxide intermediates.

Glycolate route

This method is based on the *in situ* formation of metal complexes by using chelating acetate and glycolate ligands. For this purpose, aqueous solutions or suspensions of inorganic oxides or salts are treated with diluted acetic acid at 50–60 °C to obtain clear solutions of the desired components. The metal ions present in the aqueous solutions are complexed with the help of chelating agents like poly(hydroxy alcohol) (*e.g.* ethylene glycol) or hydroxycarboxylic acid (*e.g.* citric or tartaric acid).[33–36] It is assumed that various cations are homogeneously mixed and that there is no or little segregation of the components. The mixture of complexed metal ions is heated at around 80 °C for several hours to obtain transparent solutions. The slow evaporation ($\approx$50–60 °C) of the solution initiates condensation (esterification) reactions resulting finally in a resinous gel. Subsequently, the gel is charred (300–400 °C) and calcined (1000 °C) to obtain the oxide powder. This approach had been used earlier for the successful synthesis of high-temperature superconducting oxides.[33–36] In the case of multi-component systems, the presence of an acidic medium (pH > 5) avoids the precipitation of hydroxides which may lead to compositional heterogeneities in the final material. In contrast to the metal alkoxides which can easily be purified by crystallization or distillation, the limited purity of the starting materials can play a dominant role in the elemental composition of the resulting ceramics, in this method.

Alkoxide route

Among the various solution routes for ceramic syntheses, the sol–gel technique involving hydrolysis of metal alkoxides ($M(OR)_x$) is a dominant non-fusion route to high purity ceramics.[43,44] The main features of the alkoxide-based sol–gel process are the hydrolysis and cross-condensation reactions between different metal attached alkoxy (–> M–OR) or hydroxy (–> M–OH) groups resulting in the elimination of alcohol (alcoholation) and/or water (olation) molecules. The formation of three dimensional networks by this process is associated with the chemical linking (covalent bond formation) of the metal species which favors the gelation process.

A large number of attempted syntheses and characterizations of pure yttrium and lanthanide alkoxides have reported on the formation and isolation of oxo-alkoxide clusters of general formula $M_5O(OR)_{13}$ or other 'ate' species containing undesired halide or alkali metal ions.[46–49] In view of the prevailing sceptism about the identity of simple yttrium alkoxides $Y(OR)_3$,[49] and the lack of structural evidence, the yttrium *tert*-butoxide used in this work was characterized by a single crystal X-ray diffraction analysis which has established the yttrium alkoxides as isolable and discrete species. In the solid state the molecule exists as a trimer of formula $[Y_3(OBu^t)_9(Bu^tOH)_2]$ (Fig. 1). The pertinent crystallographic data are given in Table 1. Further details on structural features are a part of an ongoing study on a series of ytttrium and lanthanide alkoxides and will be published elsewhere.[50]

Synthesis and characterization of gels and calcined powders

Method I. In the glycolate method the bimetallic (Y–Al–O) or termetallic (Y–Al–Ce–O) gels were synthesized using Y_2O_3, $Al(NO_3)_3{\cdot}9H_2O$ and $[NH_4]_2[Ce(NO_3)_6]$ as starting materials. Yttrium oxide was dissolved in 0.2 mol L^{-1} CH_3CO_2H. To this solution, a clear solution of $Al(NO_3)_3{\cdot}9H_2O$, and in the case of Ce-doped YAG, the appropriate amount of $[NH_4]_2[Ce(NO_3)_6]$, dissolved in water were added and the solution was stirred for a few hours. Finally, 1,2-ethanediol was added as a complexing agent.[36] On concentrating the solution with continuous stirring, at 60 °C, the Y–Al acetate–nitrate–glycolate solution turned into a transparent gel while the gels containing Ce were light yellow (see Experimental section).

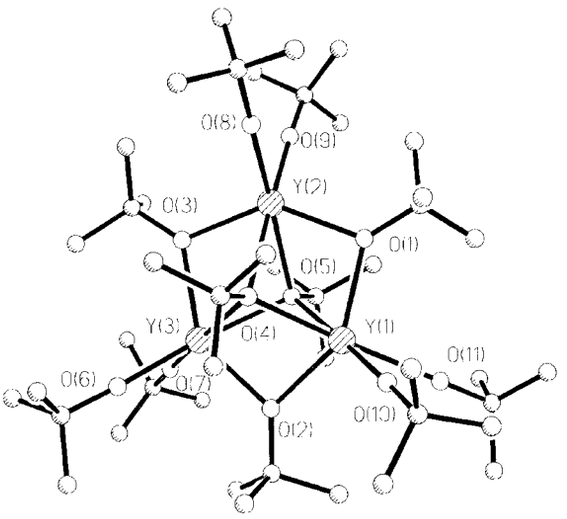

Fig. 1 Molecular structure of $[Y_3(OBu^t)_9(Bu^tOH)_2]$.

Method II. For the alkoxide based synthesis, a Pr^iOH solution of aluminium *tert*-butoxide was activated by controlled hydrolysis (alkoxide : water < 3 : 1) and a stoichiometric amount of yttrium *tert*-butoxide, dissolved in isopropyl alcohol, was added. The resulting sol was stirred for a few hours and allowed to stand overnight to obtain a transparent viscous gel. The precursor powder was obtained by removing the solvent at 50 °C at ambient pressure. During the activation, a careful monitoring of the degree of hydrolysis is essential as rapid hydrolysis can lead to the precipitation of less intractable species causing component segregation in the material. A number of examples are known where pure alkoxides of two different elements do not interact but traces of water (controlled hydrolysis!) can lead to the formation of heterometal frameworks.[46,51–53] This can be explained in the terms of the enhanced reactivity of the species in which some of the alkoxide ligands from the metal co-ordination sphere have been removed by smaller hydroxy groups. Consequently, the spatial unsaturation in the co-ordination spheres of the metals is compensated by association of different species (*via* oxo- or hydroxo-bridging) to form extended arrays.

Elemental and EDX analysis

The chemical analysis data of the precursor gels were found to be close to the starting composition (±0.5%). The initial organic contents present in the oven dried glycolate gels (Y–Al–O system: C, 20.76; H, 2.77; N, 2.36%. Y–Al–Ce–O system: C, 19.96; H, 2.83, N, 1.32%) were significantly higher than those found in the alkoxide based gels (Y–Al–O system: C, 5.20; H, 2.61%. Y–Al–Ce–O system: C, 4.96; H, 2.45%). A similar trend was found in the C and H contents of the sintered (1000 °C) YAG and Ce-doped YAG samples obtained from the glycolate (YAG: C, 1.66; H, 0.14%. Ce–YAG: C, 1.87; H, 0.05; N, 0.14%) and alkoxide (YAG: C, 0.31; H, 0.10 %. Ce–YAG: C, 0.04; H, 0.01 %) precursors. The higher percentage of carbon impurities in the glycolate route might originate from traces of undecomposed intermediates (*e.g.* yttrium carbonate or oxycarbonate) or trapped complexing agents. The average metal ratios determined by energy dispersive X-ray analysis in the sintered (1000 °C) powders and the precursor gels correspond (±1.5%) to the metal stoichiometry Y : Al = 3 : 5 consistent with the $Y_3Al_5O_{12}$ phase and in both the cases no component segregation or undesired stoichiometries were observed, at the sub-micrometer level. In the case of Ce-doped samples, a homogeneous distribution of cerium was established by high resolution electron microscopy coupled EDX analysis, performed at several spots.

Thermal behaviour

The mechanism of thermal decomposition of the dried gels was studied by TG/DTA measurements, under ambient conditions. The TG/DTA curves for gels derived from the glycolate route are shown in Fig. 2a. The TG curve shows three weight losses in the temperature ranges 20–150, 150–400 and 850–1000 °C. That below 150 °C is presumably due to evaporation of water and solvent molecules. The second and most significant decomposition step can be attributed to pyrolysis of organic compounds and degradation of intermediate species formed during the gelation process. This is in contrast to a multistep decomposition behaviour normally observed for acetate–tartrate or acetate–glycolate gels.[33–36] The third and final weight loss can be due to decomposition of trapped organic residues or small amounts of undecomposed yttrium oxycarbonate. The presence of carbonate species around 900 °C is also confirmed by the elemental analyses and IR spectrum (see below). The TG measurements clearly show that the decomposition behaviour of the Y–Al–O gel differs considerably from that of the starting materials, aluminium

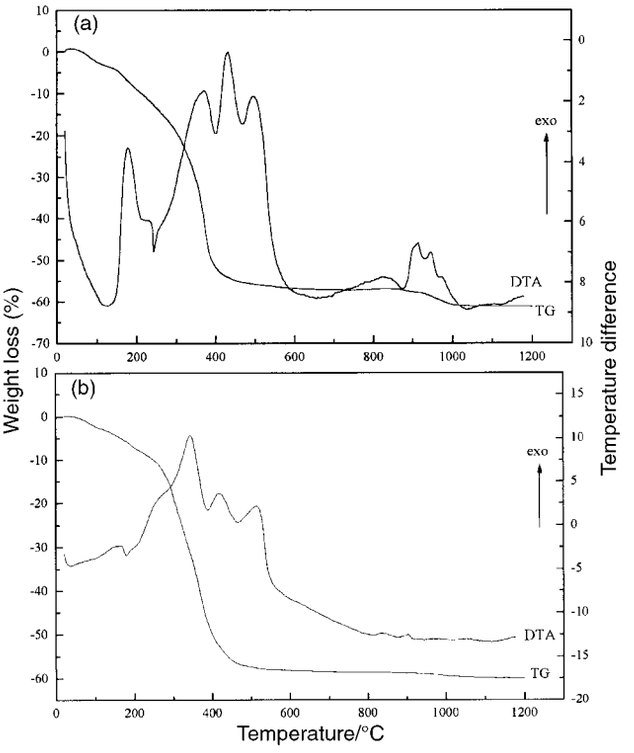

Fig. 2 TG/DTA profiles of the YAG precursor gels obtained using (a) glycolate and (b) alkoxide precursors.

nitrate and yttrium acetate. It is known that the decomposition of $Al(NO_3)_3 \cdot 9H_2O$ occurs in two steps with the main weight loss occurring around 200 °C depending on the atmosphere used (flowing air).[54] In the case of $Y(CH_3CO_2)_3 \cdot H_2O$ the dehydration process starts at 80 °C; the resulting anhydrous yttrium acetate is stable up to 300 °C ($Y_2O_2CO_3$ is also likely to be formed at this temperature), and decomposes to the oxide above 600 °C. The tendency of yttrium containing gels to react with atmospheric CO_2 is well known. The thermal decomposition behaviour associated with exothermic effects in the DTA curve indicates an autoignited combustion process[34] arising, probably, from exothermic anionic oxidation–reduction reactions between glycolate, acetate and nitrate ions. Since the structures of the gel complexes are not known, a more detailed interpretation of the decomposition mechanism is complicated. A number of closely associated exothermic features above 850 °C can arise from the decomposition of trapped carbonaceous residues as well as the beginning of crystallization and accompanying structural transformations. Yttrium hydroxide is known readily to absorb carbon dioxide from the atmosphere as indicated by the presence of IR stretches corresponding to the CO_3^{2-} group, in gels sintered at 800–900 °C (see later).

Fig. 2b shows the TG/DTA curves for the Y–Al–O gel synthesized by the alkoxide route. In comparison to the glycolate synthesis, the weight loss of the alkoxide derived gel occurs in two steps. The first (100–300 °C) corresponds possibly to removal of adsorbed and chemically bonded water and alcohol molecules. The second and main decomposition (300–550 °C) can be attributed to elimination of alkoxy groups (alcoholation) attached to different metal centers of the molecular precursor which is supported by the two exotherms present in this region. In contrast to the glycolate gels, no carbon dioxide incorporation and decomposition of carbonate species was observed during the calcination and sintering of alkoxide gels which is also indicated by the relatively featureless (above 600 °C) nature of the TG curve. The small exotherms in the range 770–810 °C indicate the crystallization of the YAG

phase which is also confirmed by XRD measurements on the sample heat treated at 700 °C. No significant weight loss is observed thereafter indicating the formation of an oxide of definite composition. The difference in the crystallization temperatures observed by DTA and XRD analysis is possibly due to the fact that in the case of DTA analysis samples were heated at a rate of 5 °C min^{-1} whereas the sintering time for the powders was 6 h.

Infrared spectra

The IR spectra of the Y–Al–O gel and sintered powder prepared by the glycolate route are presented in Fig. 3. The bands observed may be divided into four regions: 3750–2850, 1700–1300, 1150–950 and 800–450 cm^{-1}. The bands due to the CH_3 and CH_2 stretching frequencies are observed at 2960–2850 and 1430–1420 cm^{-1},[55,56] whereas the intense and broad envelope of bands at 3550–3200 cm^{-1} is due to the overlapping of hydroxyl stretches of free glycol ([CH_2]–OH) and the ν(OH) frequencies of the water of crystallization, present in the gels. The C(O)–OH stretching frequencies can be identified at 3300–2850, 1640–1600, 1340–1290 and 1050–1000 cm^{-1}. A series of bands in the ranges 1700–1650, 1480–1450 and 940–910 cm^{-1} can be assigned to the nitrate groups. Thus, it is not possible to state that only one precursor compound was formed, however the IR, TG and elemental analyses of the gels show the 1,2-ethanediol and nitrate ligands to be present in the metal co-ordination spheres. As evident in the IR spectra, no carbonate groups are present in the oven-dried gels and the calcined (500 °C) powder. However, the appearance of a carbonate stretching frequency (1750–1795 cm^{-1}) for samples calcined at 900 °C is caused by the reaction of CO_2 expelled during the combustion of trapped organic impurities or due to the absorption of atmospheric CO_2 while cooling.[57] The presence of carbonate at this temperature is also supported by the elemental analysis which shows a significant amount of carbon (1.66%) and negligible hydrogen (0.14%) and nitrogen (0.05%) contents. The absence of nitrogen is also evident in the disappearance of nitrate stretching frequencies (Fig. 3). The peaks at 771, 686, 644 and 495 cm^{-1} represent the characteristic metal–oxygen vibrations.[58–60]

Fig. 4 shows the FTIR spectra of the gels and sintered YAG and Ce–YAG ceramics obtained from alkoxide precursors. The gel spectra were comparable in both cases exhibiting broad hydroxyl stretches from 3000 to 3400 cm^{-1}. The peaks in the regions 3000–2800 and 1100–1600 cm^{-1} can be assigned to C–H and C–O stretches, respectively, arising from metal-attached alkoxy groups.[38] Additionally, the bridging and terminal (C–OM) (M = Al or Y) stretching frequencies are observed in this region. The heat treated samples show only metal–oxygen vibrations which in accord with earlier

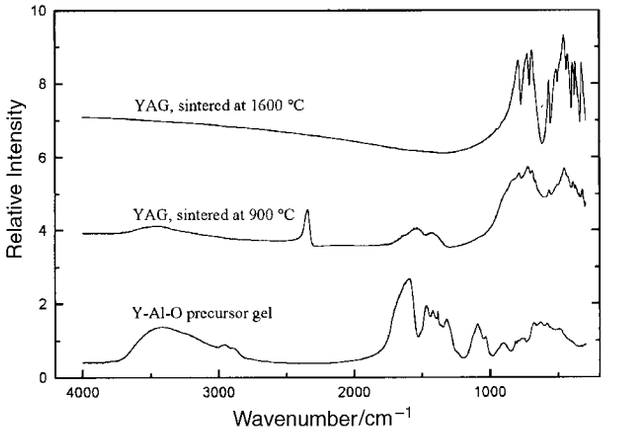

Fig. 3 FT-IR spectra of the YAG precursor gel and the sintered (1000 °C) ceramic (glycolate route).

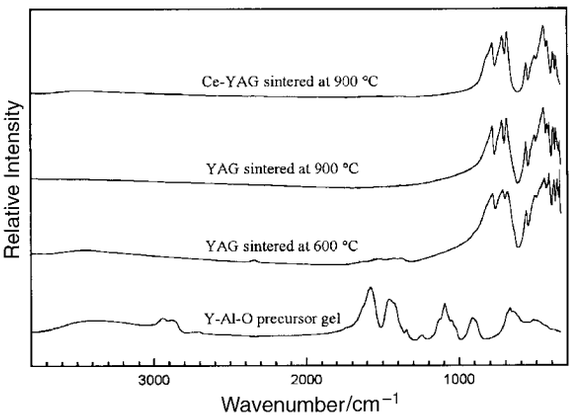

Fig. 4 FTIR spectra of the precursor gels and the sintered (900 °C) YAG and Ce-doped YAG ceramics (alkoxide route).

reports are characteristic of Y–O and Al–O stretching frequencies.[55–57,59] The Ce^{3+}–YAG sample (Fig. 4) does not show IR frequencies corresponding to other phases [*e.g.* Ce_2O_3, Y_2O_3, (Ce/Y)AlO_3], however a small shift with respect to the YAG peaks is observed. This observation suggests that Ce is statistically well dispersed in the YAG lattice, which is also supported by the XRD data (see later).

Powder X-ray diffraction studies

The XRD patterns of the Y–Al–O precursor (glycolate synthesis) calcined and sintered at different temperatures between 800 and 1600 °C are shown in Fig. 5a. The pattern of the powder obtained at 800 °C (8 h) shows the coexistence of other crystalline phases (*e.g.* $Y_2Al_4O_9$, $YAlO_3$) which are transformed at higher temperature (> 900 °C) into $Y_3Al_5O_{12}$. The diffractogram at 1000 °C showed all the peaks corresponding to the YAG phase (JCPDS file [33-40])[61] (Fig. 5a). Further heat treatment in the range 1200–1600 °C indicated that still insignificant crystallization occurs, however no thermal degradation or crystallization of any undesired or contaminating phase could be identified.

Fig. 5b shows the X-ray diffraction patterns of the heat treated YAG precursor powder obtained from the alkoxide route. The XRD patterns of the samples sintered below 600 °C exhibit broad peaks indicative of incipient crystallization and the presence of short-range ordering. Also, the IR spectra (Fig. 4) reveal that the local environment is possibly YAG but higher temperatures are essential for the structure evolution. At 700 °C the XRD pattern shows YAG to be the only crystalline component, this is the lowest reported temperature for the formation of single phase crystalline YAG material. In contrast to the glycolate synthesis, no other crystalline phases were formed on using alkoxide precursors. In the other solution synthesis of YAG[19–23] the crystallization was reported to begin above 900 °C and the other metastable yttrium aluminate phases were observed at temperatures below 1000 °C. The monophasic YAG ceramic was observed only at higher temperatures (1200–1600 °C). The XRD patterns of the material sintered at 800 and 1000 °C (Fig. 5b) show sharper profiles corresponding to the continuation of the crystallization process and crystallite growth. This observation is thoroughly supported by high resolution electron microscopy studies (see later). For a comparative evaluation of solution and solid state syntheses, the XRD profile of the material obtained by thermolysis (1000 °C, 24 h) of a physical mixture of aluminium nitrate and yttrium oxide is reproduced in Fig. 5c which shows the presence of several species other than the desired YAG phase (JCPDS file [33-40]).[61]

The XRD patterns of the Ce–YAG ceramics are shown in Fig. 6. The first signs of crystallization were observed, in both

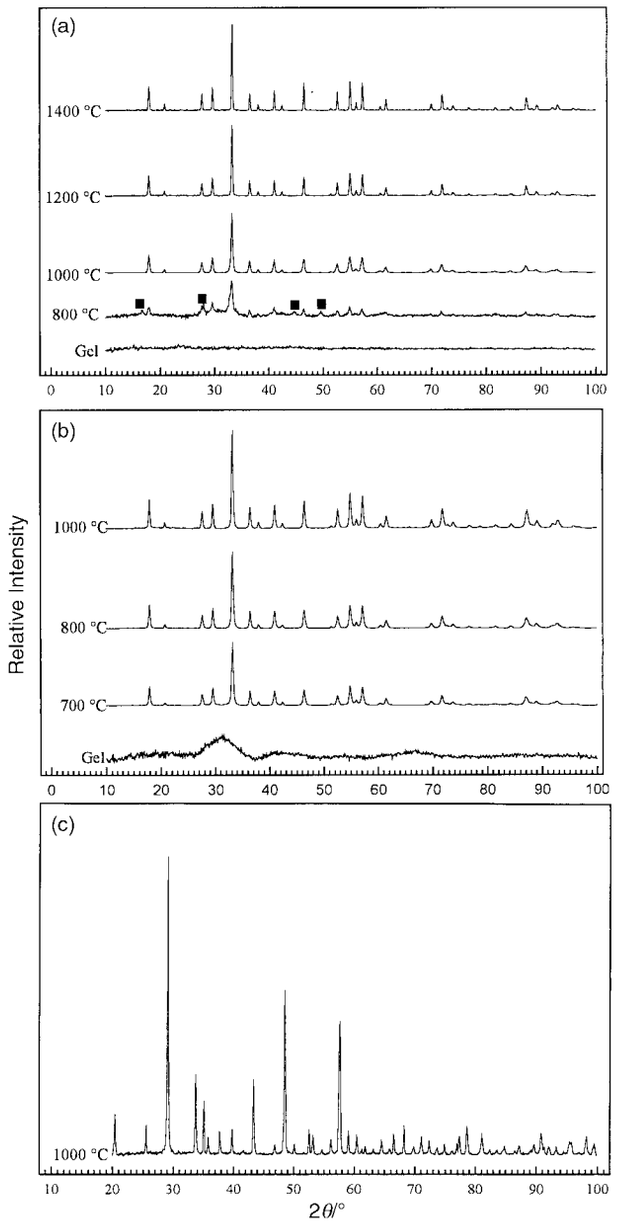

Fig. 5 Temperature dependent XRD traces of the ceramic obtained using (a) glycolate, (b) alkoxide and (c) solid state routes. The peaks other than those of the YAG phase in the case of glycolate synthesis (800 °C) are marked (■).

cases, at temperatures higher than those required for undoped YAG ceramics. The alkoxide synthesis gave a well developed Ce-doped garnet phase at 800 °C while a crystalline Ce-doped YAG phase was observed at 1000 °C in the case of glycolate synthesis (Fig. 6). In both cases the peak pattern corresponds to the characteristic YAG pattern (JCPDS file [33-40]) and no formation of the crystalline dopant oxide CeO_2 was observed, till 1000 °C. Further, the IR spectra of the calcined samples show no extra peaks or features when compared with the spectra of pure YAG ceramic (Fig. 4). Also, the EDX data of the doped samples exhibit no heterogeneity with respect to the distribution of cerium.

^{27}Al NMR spectroscopy

The sensitivity of magic angle spinning (MAS) ^{27}Al NMR chemical shifts towards the co-ordination state of Al^{III} is increasingly being used for identifying the different phases and co-ordination states of Al centers in aluminium containing materials.[62,63] The ^{27}Al MAS NMR spectra of the different gels

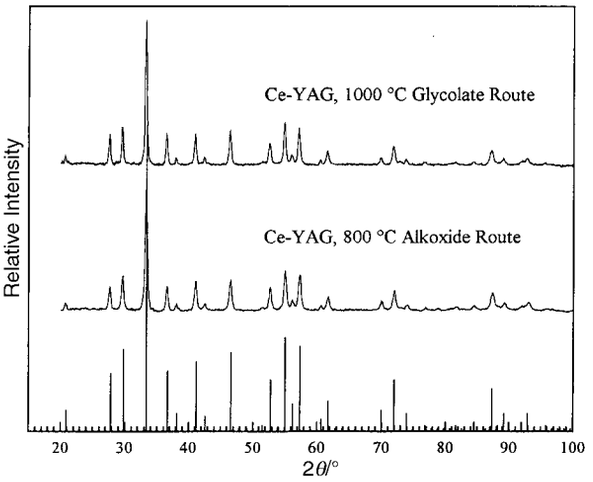

Fig. 6 XRD traces of Ce-doped YAG ceramics obtained by glycolate (a) and alkoxide (b) routes. The vertical lines correspond to the JCPDS ([33-40]) indexing.

and calcined samples are presented in Fig. 7 and 8. The solid-state structure of $Y_3Al_5O_{12}$ consists of a network of four- and six-fold co-ordinated aluminium atoms. The yttrium atoms reside in the dodecahedral interstices formed by the corner-sharing arrangement of the AlO_4 and AlO_6 polyhedra. The ^{27}Al NMR spectrum (Fig. 7a) of the Y–Al–O gel (glycolate route) shows a sharp signal (δ 0.93) in the region characteristic of six-co-ordinate aluminium(III) centers along with a broad peak, which overlaps with the first order side bands, suggesting the probable presence of four-co-ordinated Al. On the contrary, the NMR spectrum (Fig. 7b) of Y–Al–O gel (alkoxide route) shows two distinct resonances at δ 1.40 and 36.07 which correspond to six-(AlO_6) and five-(AlO_5) co-ordinated aluminium sites (Fig. 7b). This observation suggests the initial gel structures to be different in the two synthetic approaches. The

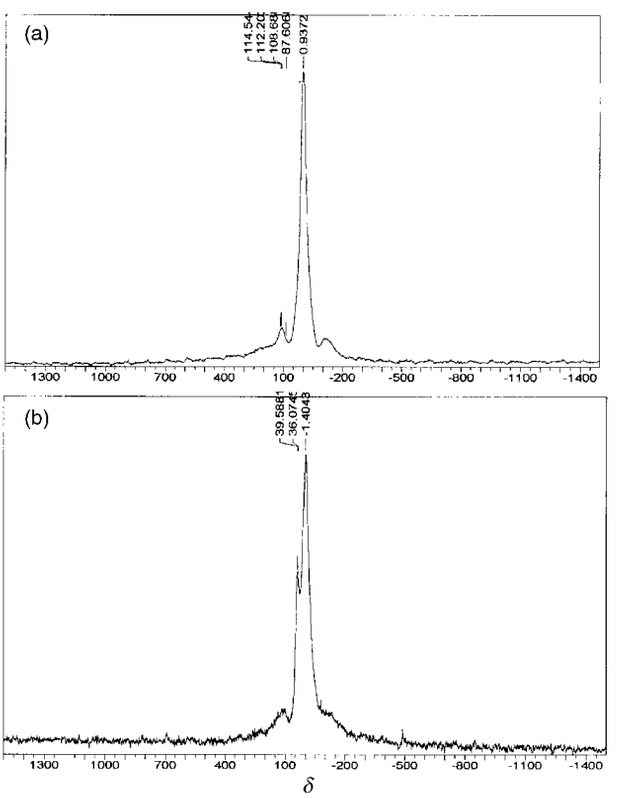

Fig. 7 ^{27}Al CP MAS NMR spectrum of the gel powder obtained by (a) glycolate and (b) alkoxide routes.

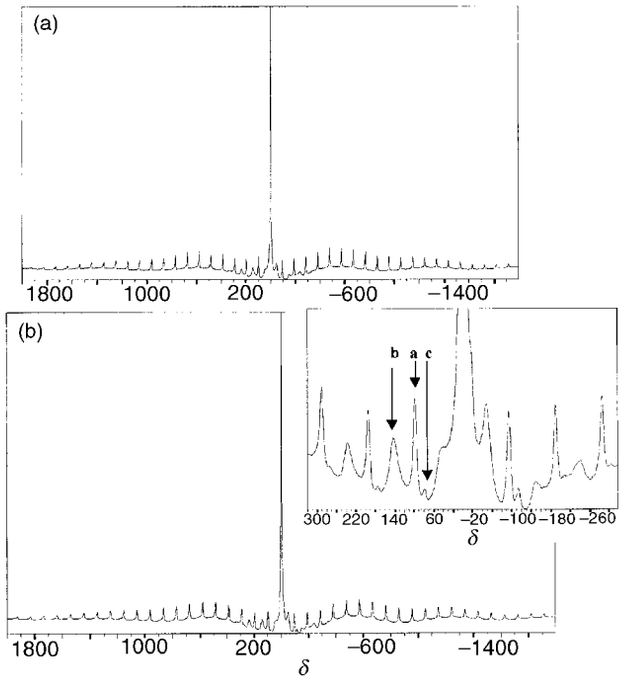

Fig. 8 ^{27}Al CP MAS NMR spectrum of the Ce–YAG ceramic sintered at 900 °C obtained *via* (a) glycolate and (b) alkoxide routes. a, b and c (in the inset) represent the three different families of satellite spinning side bands.

^{27}Al NMR spectral features (Fig. 8a and 8b) of the calcined samples, in both cases, reveal a sharp signal flanked by intense spinning side bands for octahedral aluminium. The presence of four-fold co-ordinated aluminium species ($\delta \approx 60$) is clearly evident in the asymmetric nature of the first order side bands and the appearance of side bands corresponding to AlO_4 (Fig. 8a). The disappearance of five-co-ordinate aluminium(III) species in the sintered alkoxide gels suggest the migration of aluminium ions into tetrahedral or octahedral holes. This phenomenon is frequently observed in the thermal evolution of transitional aluminas. In the case of the Ce-doped sample (alkoxide route), besides the spectral feature of the pure YAG ceramics, three distinct sets of satellite spinning side bands (marked as a, b and c in the inset of Fig. 8b) were observed at ≈ 40 ppm intervals which suggests the presence of three aluminium(III) centers in chemically different environments. The two distinct peaks in the region characteristic[63] of octahedral aluminium represent two six-fold co-ordinated aluminium centers which are magnetically inequivalent. In view of the relative intensities of the peaks, the small peak might arise from the AlO_6 units experiencing the chemical influence of the dopant cerium ions. The possibility of alumina or any other aluminate being present can be ruled out in the light of XRD data and the extremely crystalline nature of the material.

Scanning and transmission electron microscopy

The typical scanning electron micrographs of the glycolate derived gel consist of agglomerates with a highly porous structure while more faceted grains were observed in the case of alkoxide synthesis. The SEM images of calcined alkoxide gels show non-agglomerated grains with a defined and regular micro-structure whereas the sintered glycolate powders consist of a multi-modal mixture of crystallites (Fig. 9). The SEM image of Ce–YAG (Fig. 10), calcined at 1000 °C, revealed grains ranging from 5 to 15 μm with a morphology similar to that observed for pure YAG samples. The TEM image (Fig. 11) of YAG ceramic (alkoxide route), sintered at 700 °C, shows dispersed crystallites of nearly uniform size

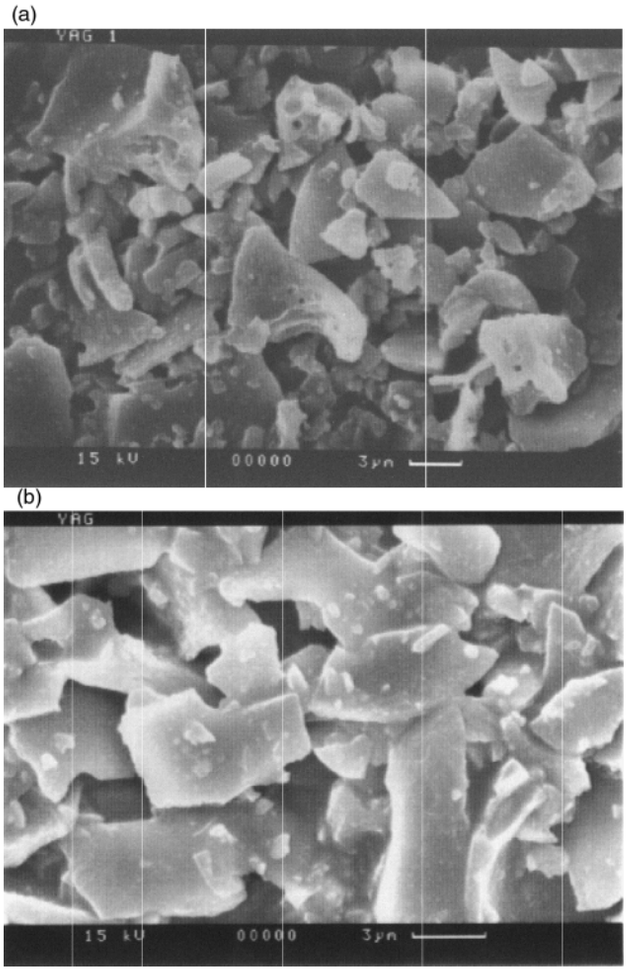

Fig. 9 Scanning electron micrograph of $Y_3Al_5O_{12}$ sintered at 1000 °C: (a) glycolate and (b) alkoxide route.

(60–80 nm). On the other hand, the TEM images of YAG powders sintered at higher (1000 °C) temperature showed (Fig. 12) aggregation of crystallites which is significantly higher in the glycolate-derived samples. Besides the particle agglomeration caused by the higher sintering temperatures, the enhanced clustering tendency of the particles in the case of glycolate synthesis may be due to the decomposition (>900 °C) of yttrium carbonate or oxycarbonate species or traces of the unburnt complexing agents (which may function as binders) as also indicated by the higher amount of carbon present in the

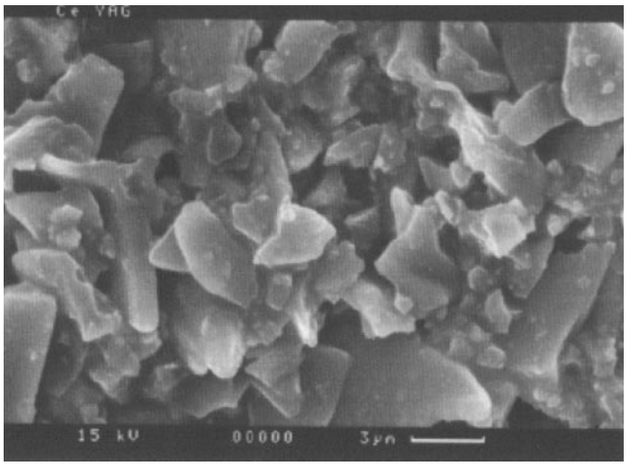

Fig. 10 Scanning electron micrograph of the Ce-doped YAG sintered at 1000 °C.

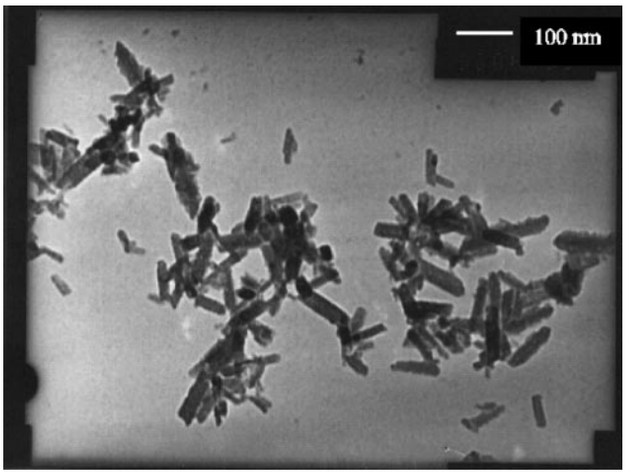

Fig. 11 Transmission electron micrograph of a YAG sample obtained by the alkoxide route, after calcination at 700 °C.

samples (see above). The grain growth during sintering is a well known effect, the driving force being the reduction of grain boundary area and thus the total energy of the system. Fig. 13a shows the fusion of small YAG crystallites to form dumb-bell shaped particles which grow further to form clusters of grains. The HREM lattice image (Fig. 13b) shows a sinter-neck of two nano-YAG particles which have different crystallographic orientation to each other. The lattice parameters of the high resolution images, measured from the FFT (Fast Fourier Transform) of the real image, correspond to the YAG phase (JCPDS [33-40]). The grain structure and texture of the Ce–YAG sample (Fig. 14) observed in transmission electron micrographs were similar to the pure YAG ceramics which supports the IR and XRD observations where no other phase (*e.g.* $(Ce,Y)AlO_3$) was detected.

X-Ray photoelectron spectroscopy

The XPS surface measurements were performed on pure and Ce-doped YAG samples (pellets of thickness 2 mm) to control the elemental composition and the chemical state of the dopant cerium ions. The overview XPS spectra of the two YAG samples prepared by glycolate and alkoxide routes are shown in Fig. 15. The results revealed the presence of yttrium and aluminium in the expected stoichiometry ($Y:Al=1.67$), in both cases. The spectra showed no extraordinary features except higher carbon contamination in the sample obtained by the glycolate route, a fact borne out by the elemental analysis of the sintered powders (see above). In the case of Ce-doped samples, the spectral features that are characteristic of either Ce^{3+} or Ce^{4+} species have been used to identify the chemical state of cerium in the samples. The XPS Ce 3d spectra of cerium compounds are known to be complex due to hybridization of the Ce 4f with ligand orbitals and fractional occupancy of the valence 4f orbitals. The XPS spectrum (Fig. 16) of Ce^{3+}(5%)–YAG (alkoxide route) showed only two sets of doublets which according to previous studies[64–66] is consistent with a +3 oxidation state of cerium. Since the samples were sintered under ambient conditions, oxidation of cerium-(III) species to -(IV) species was expected but not detected even after long analysis time. Interestingly, the XPS Ce 3d spectrum (Fig. 16) of the Ce^{4+}(8%)–YAG sample also showed four peaks ($3d_{5/2}$ at −881.6 and −885.6; $3d_{3/2}$ at −899.9 and −904.2 eV) characteristic of Ce^{3+} while the identifying feature of Ce^{4+} (highest binding energy peak at −917 eV)[64–66] was not observed even with short analysis time periods and an *in situ* scraping of the surface with a diamond file. The photoreduction of cerium oxide ($Ce^{4+}\rightarrow A\%Ce^{4+}+B\%Ce^{3+}$; $A\neq 0$) under the conditions used for XPS measurements is well known and attributed primarily to the intense heating of the sample surface.[67] We have attempted to limit the photoreduction by controlling the X-ray beam power and irradiation time, however no Ce^{4+} feature was observed (Ce^{4+}–YAG) even with short analysis time on freshly scraped surfaces. Since no evidence for the formation of a new phase was observed in the XRD data, we assume that the dopant CeO_2 (glycolate synthesis) was reduced, during the heat treatment, to Ce_2O_3 creating an oxygen vacancy for each pair of Ce^{4+} ion, (eqn. 1). This observation is

$$2CeO_2\rightarrow Ce_2O_3+1/2\ O_2 \qquad (1)$$

in accordance with the reported redox reactions of cerium(IV) oxide during the high temperature sintering process.[68] Further, it is known for doped garnet materials that the charge imbalance caused due to the different valency of dopant ions (than the host cations) is compensated by oxygen vacancies.[69] The valence XPS spectra (Fig. 17) of pure and doped samples show a broad envelope with two features (between −34 and −16 eV) corresponding to O 2s and Y 4p peaks, respectively. On constraining the two data sets with a constant total integrated O 2s intensity, it becomes evident that the intensity of the Y 4p peak has decreased, for the Ce-doped sample. This

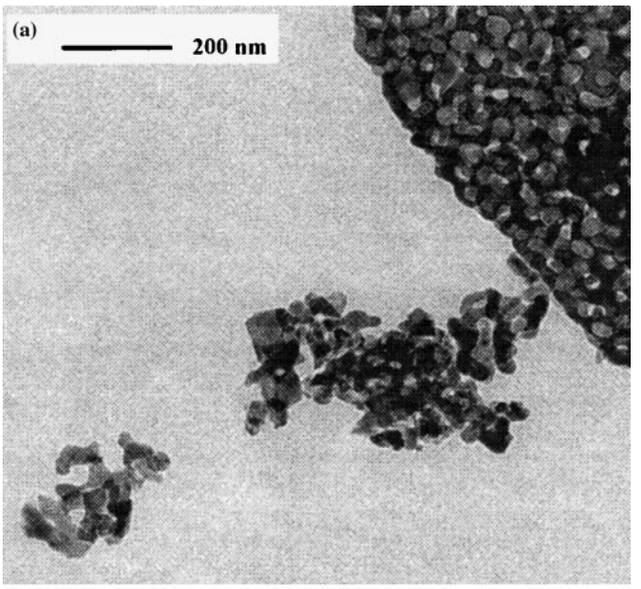

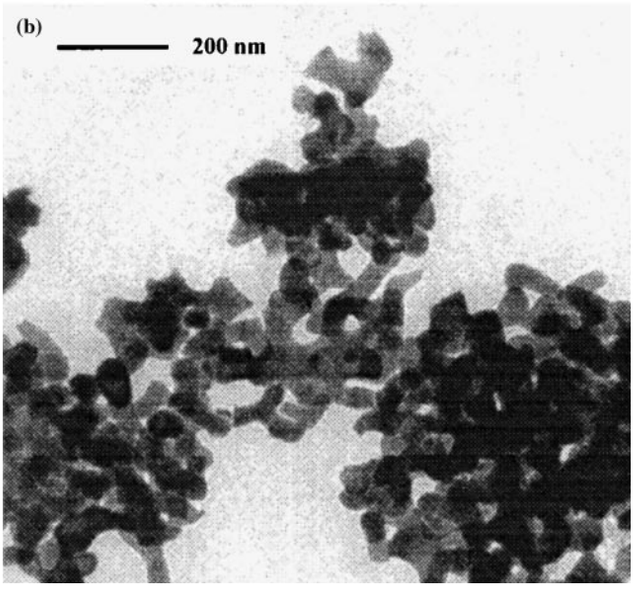

Fig. 12 Transmission electron micrographs of YAG ceramic, sintered at 1000 °C: (a) glycolate and (b) alkoxide route.

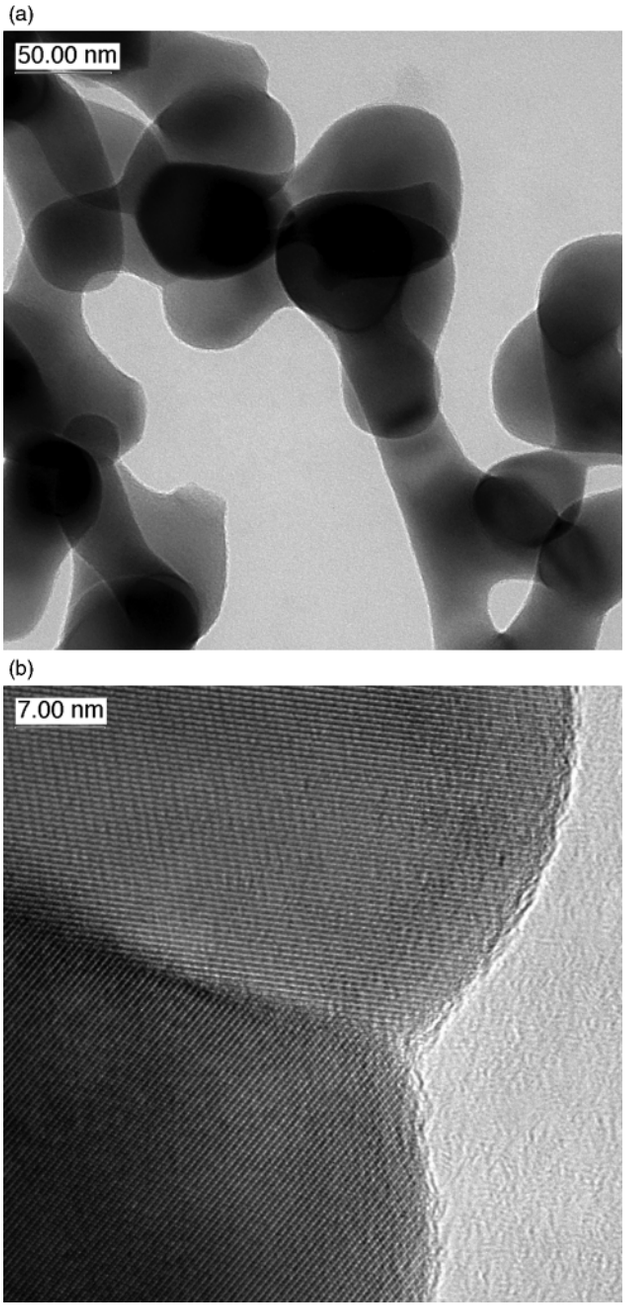

Fig. 13 HRTEM image of a YAG specimen, sintered at 1000 °C (alkoxide route). The fusion of YAG crystallites to form agglomerates is evident in the lattice image which shows a sinter-neck of two nano-YAG particles.

suggests the possible substitution of Y^{3+} by Ce^{3+} ions. The Y 4p peak due to excess Y_2O_3 (upon substitution) is expected at lower binding energy but was not detected probably due to overlapping with the much larger O 2s band. Alternatively, the small amount of yttria is located between the grain boundaries and could not be detected effectively due to the surface sensitive nature of the ESCA method (probing depth 10–20 Å).

Conductivity measurements

The electrical conductivity measurements were performed on the compacts of YAG (<100 nm) which is known to be a typically high resistance material. In contrast to the expected dielectric behaviour, the resistivity values of the examined specimens (glycolate synthesis) increased gradually till 50 and 60 °C for the pure and Ce-doped YAG, respectively. Above these temperatures a resistivity jump of the order 10^2 Gohms is observed (Fig. 18). The values of electrical conductivity (σ) fall

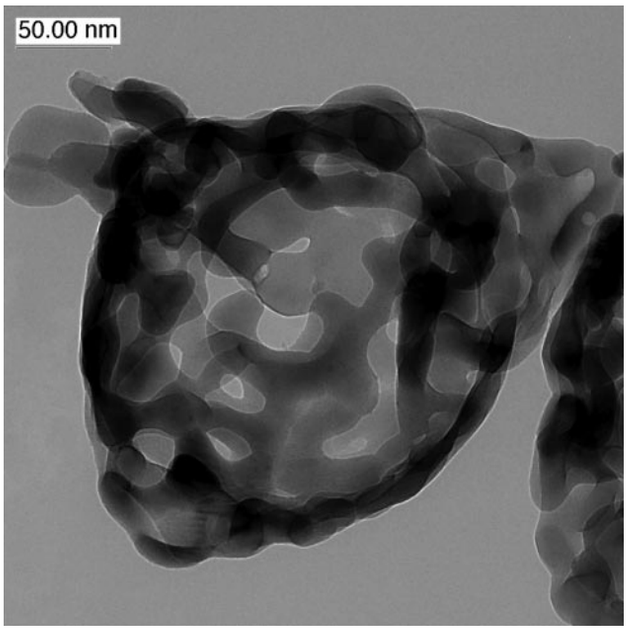

Fig. 14 TEM image of a sintered (1000 °C) Ce-doped YAG ceramic obtained from the glycolate route.

in the range 10^{-14}–10^{-16} ohm^{-1} cm^{-1} for the temperature range 20–160 °C. This unusual behaviour is not unattended in the nanocrystalline oxides and is largely attributed to the contribution of individual crystallites in the nano-grained substances. Also, the presence of foreign substances within the grain boundaries can not be ruled out. The observed high resistivity values at higher temperature might result from trapping of charge carriers in the grain boundaries. It has been reported for yttria stabilized tetragonal zirconia that compacts with crystallite size less than 50 nm show semi-conducting properties whereas those with crystallite size more than 50 nm show a quasi-metallic behaviour.[70] Another noticeable feature is the high dielectric strength of the samples,[71] *i.e.* they withstand high voltages (>1000 V) without undergoing any degradation or becoming electrically conducting. Also, the Ce–YAG sample exhibits a similar behaviour (Fig. 18) which rules out the possibility of dopant (Ce^{4+}) ions being present as mobile charge carriers. This is also supported by the XPS studies which define the oxidation state of cerium as +3.

Conclusion

Homogeneous gels achieved either by controlled hydrolysis of alkoxide precursors or by complexation of metal ions with 1,2-

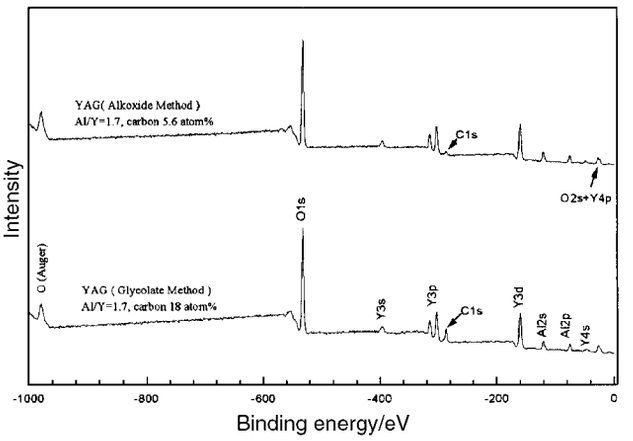

Fig. 15 Overview XPS spectra of the YAG samples prepared by the two different methods.

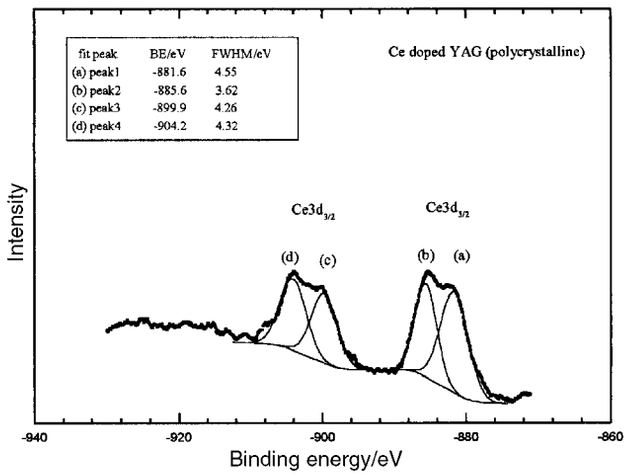

Fig. 16 The Ce 3d core level XPS spectrum in the Ce^{4+}-doped YAG specimen (glycolate synthesis).

ethanediol in an aqueous medium have been used for the low-temperature synthesis of nano-scaled yttrium aluminium garnet (YAG, $Y_3Al_5O_{12}$). The present study demonstrates the versatility of solution methods to yield monophasic YAG samples at lower sintering temperatures (700 °C (alkoxide route) or 1000 °C (glycolate route)) when compared to the temperature required for the solid-sate synthesis (>1600 °C). Although several wet-chemical techniques have been employed for obtaining $Y_3Al_5O_{12}$, the coexistence of other phases like $YAlO_3$ and $Y_2Al_4O_9$ was invariably observed below 1000 °C. The successful synthesis of crystalline YAG phase at 700 °C, in this work, is the lowest reported temperature for the crystallization of this material. With respect to the phase purity of powders both methods gave comparable results, however the crystallization temperatures and residual carbon contents for alkoxide derived powders were significantly lower. The gross microstructural features of the two YAG specimens were quite similar but the products obtained from glycolate synthesis show higher agglomeration effects. However, the sol–gel method in aqueous media is less expensive and thus appropriate for the large scale production of YAG ceramics. Also, Ce-doped YAG ceramics have been successfully obtained by both methods. Attempts to incorporate Ce^{4+} as dopant ions in the YAG lattice gave only Ce^{3+}–YAG probably due to the thermal reduction of cerium(IV) species during the sintering process. Recent studies have shown that highly transparent YAG ceramics with optical transmittance comparable with YAG single crystals could be obtained from compacts of polycrystalline $Y_3Al_5O_{12}$.[7] In view of the above and the

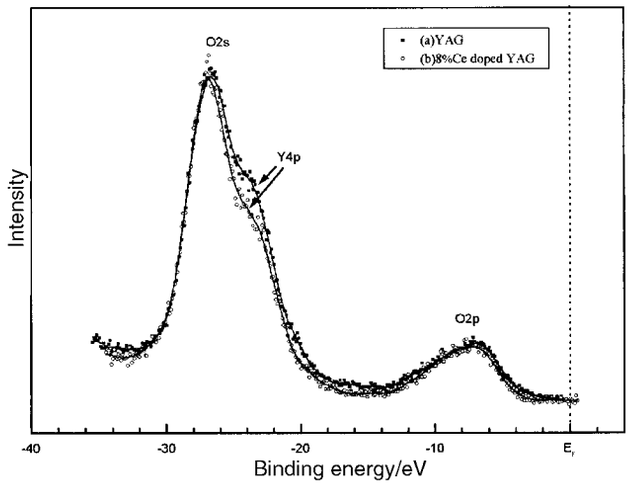

Fig. 17 XPS valence spectra of the YAG and Ce-doped YAG samples.

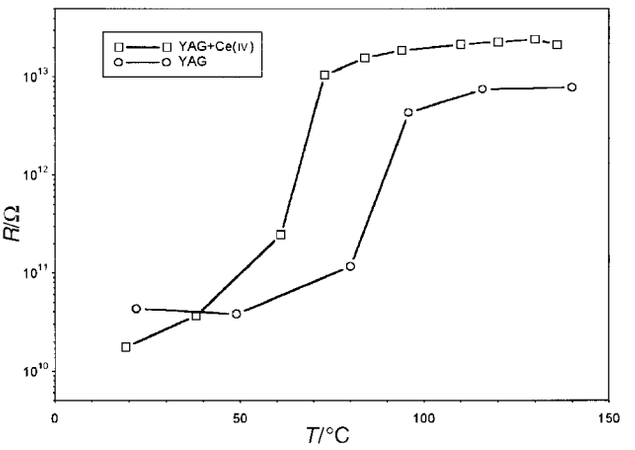

Fig. 18 Electrical conductivity of the YAG and Ce–YAG ceramics sintered at 1000 °C (glycolate route).

increasing importance of nanomaterials, the nanocrystalline YAG and doped YAG phases show considerable application potential. Our studies on the synthesis and characterization of lanthanide doped YAG and the effect of dopant concentration on the optical properties are currently underway.

Acknowledgements

The authors thank the Deutsche Forschungsgemeinschaft for financial support in the framework of the research programme Sonderforschungsbereich 277 at the University of Saarland, Saarbruecken. The Volkswagen and Alexander von Humboldt Foundations are gratefully acknowledged for fellowships to A.K. and S.M., respectively. We are thankful to Prof. S. Hüfner and Mr. Shen Hao for X-ray photoelectron spectroscopy.

References

1 J. E. Geusic, H. M. Marcos and L. G. van Uitert, *Appl. Phys. Lett.*, 1964, **4**, 182.
2 J. Machan, R. Kurtz, M. Bess and M. Birnbaum, *J. Opt. Soc. Am.*, 1987, **20**, 134.
3 A. P. Shkadarevich, *J. Opt. Soc. Am.*, 1989, **22**, 60.
4 T. Izumitani, *Bull. Ceram. Soc. Jpn.*, 1991, **26**, 108.
5 A. Ikesue, K. Kamata and K. Yoshida, *J. Am. Ceram. Soc.*, 1995, **78**, 2545.
6 A. Ikesue, K. Yoshida and K. Kamata, *J. Am. Ceram. Soc.*, 1996, **79**, 507.
7 B. Anvari, B. S. Tanenbaum, W. Hoffman, S. Said, T. E. Milner, L. H. L. Liaw and J. S. Nelson, *Phys. Medic. Biol.*, 1997, **42**, 265.
8 A. H. Chokshi and J. R. Porter, *J. Am. Ceram. Soc.*, 1986, **69**, C-37.
9 T. A. Parthasarathy, T. Mah and K. Keller, *Ceram. Eng. Sci. Proc.*, 1991, **12**, 1767.
10 G. S. Corman, *Ceram. Eng. Sci. Proc.*, 1991, **12**, 1745.
11 G. S. Corman, *J. Mater. Sci. Lett.*, 1993, **12**, 379.
12 B. H. King, Y. Liu, R. Laine and J. W. Halloran, *Ceram. Eng. Sci. Proc.*, 1993, **14**, 639.
13 G. N. Morscher, K. C. Chen and K. S. Mazdiyasni, *Ceram. Eng. Sci. Proc.*, 1994, **15**, 181.
14 T. Rouxel, J. F. Baumard, J. L. Besson, F. Valin and M. Boncoeur, *Eur. J. Solid State Inorg. Chem.*, 1995, **32**, 617.
15 W. R. Blumenthal and D. S. Phillips, *J. Am. Ceram. Soc.*, 1996, **79**, 1047.
16 J.-M. Yang, S. M. Jeng and S. Chang, *J. Am. Ceram. Soc.*, 1996, **79**, 1218.
17 A. Kareiva, C. J. Harlan, D. B. MacQueen, R. L. Cook and A. R. Barron, *Chem. Mater.*, 1996, **8**, 2331.
18 J. L. Bates and J. E. Garnier, *J. Am. Ceram. Soc.*, 1981, **64**, C-138.
19 B. H. King and J. W. Halloran, *J. Am. Ceram. Soc.*, 1995, **78**, 2141.
20 Y. Liu, Z.-F. Zhang, B. King, J. Halloran and R. M. Laine, *J. Am. Ceram. Soc.*, 1996, **79**, 385.
21 A. M. George, N. C. Mishra, M. S. Nagar and N. C. Jayadevan, *J. Therm. Anal.*, 1996, **47**, 1701.

22 M. Yada, M. Ohya, M. Machida and T. Kijima, *Chem. Commun.*, 1998, 1941.
23 C. J. Harlan, A. Kareiva, D. B. MacQueen, R. Cook and A. R. Barron, *Adv. Mater.*, 1997, **9**, 68.
24 G. Gowda, *J. Mater. Sci. Lett.*, 1986, **5**, 1029.
25 R. S. Hay, *J. Mater. Res.*, 1993, **8**, 578.
26 R. Manalert and M. N. Rahaman, *J. Mater. Sci.*, 1996, **31**, 3453.
27 M. Veith, S. Mathur and C. Mathur, *Polyhedron*, 1998, **17**, 1005.
28 M. Veith and S. Kneip, *J. Mater. Sci. Lett.*, 1994, **13**, 335.
29 M. Veith, S. Faber, R. Hempelman, S. Janssen, J. Prewo and H. Eckerlebe, *J. Mater. Sci.*, 1996, **31**, 2009.
30 M. Veith, S. Kneip, A. Jungmann and S. Hüfner, *Z. Anorg. Allg. Chem.*, 1997, **623**, 1507.
31 M. Veith, A. Altherr, N. Lecerf, S. Mathur, K. Valtchev and E. Fritscher, *Nanostr. Mater. Proc. NANO*, 1999, **98**, 191.
32 M. Veith, A. Altherr and H. Wolfanger, *Adv. Mater.*, 1999, **5**, 87.
33 A. Kareiva, M. Karppinen and L. Niinistö, *J. Mater. Chem.*, 1994, **4**, 1267.
34 I. Bryntse and A. Kareiva, *Physica C*, 1995, **251**, 115.
35 M. K. Van Bael, E. Knaepen, A. Kareiva, I. Schildermans, R. Nouwen, J. D'Haen, M. D'Olieslaeger, C. Quaeyhaegens, D. Franco, J. Yperman, J. Mullens and L. C. Van Poucke, *Supercond. Sci. Technol.*, 1998, **11**, 82.
36 A. Kareiva, I. Bryntse, M. Karppinen and L. Niinistö, *J. Solid State Chem.*, 1996, **121**, 356.
37 M. F. Lappert, P. P. Power, A. R. Sanger and R. C. Srivastava, *Metal and Metalloid Amides*, Wiley & Sons, New York, 1980
38 D. C. Bradley, R. C. Mehrotra and D. P. Gaur, *Metal Alkoxides*, Academic Press, London, 1978.
39 G. M. Sheldrick, (*a*) SHELXS 86, Program for Crystal Structure Determination, University of Göttingen, 1986 ; (*b*) SHELXL 97, Program for Crystal Structure Determination, University of Göttingen, 1997.
40 R. C. Mehrotra, *Chemtracts*, 1990, **2**, 338.
41 C. D. Chandler, C. Roger and M. Hampden-Smith, *J. Chem. Rev.*, 1993, **93**, 1205.
42 D. L. Segal, *Chemical Synthesis of Advanced Materials*, Cambridge University Press, Cambridge, 1989.
43 C. J. Brinker and G. W. Scherrer, *Sol–Gel Science: The Physics and Chemistry of Sol–Gel Processing*, Academic Press, New York, 1990.
44 L. L. Hench and J. K. West, *Chem. Rev.*, 1990, **90**, 33.
45 D. L. Segal, *J. Mater. Chem.*, 1997, **7**, 1297.
46 R. C. Mehrotra and A. Singh, *Chem. Soc. Rev.*, 1996, 1.
47 O. Poncelet, W. J. Sartain, L. G. Hubert-Pfalzgraf, K. Folting and K. G. Caulton, *Inorg. Chem.*, 1989, **28**, 263.
48 D. C. Bradley, H. Chudzynska, D. M. Frigo, M. E. Hammond, M. B. Hursthouse and M. A. Mazid, *Polyhedron*, 1990, **9**, 719.
49 R. C. Mehrotra, A. Singh and U. M. Tripathi, *Chem. Rev.*, 1991, **91**, 1287.
50 S. Mathur and M. Veith, unpublished work.
51 G. J. Westin, *Sol–Gel Sci. Technol.*, 1999, **13**, 125.
52 M. Veith, S. Mathur, V. Huch and T. Decker, *Eur. J. Inorg. Chem.*, 1998, 1327.
53 M. Veith, S. Mathur, N. Lecerf, V. Huch, T. Decker, H. P. Beck, W. Eiser and R. Haberkorn, *J. Sol–Gel Sci. Technol.*, 1999, in the press.
54 A. Kareiva, unpublished work.
55 P. S. Devi and H. S. Maiti, *J. Solid State Chem.*, 1994, **109**, 35.
56 K. Nakanishi, *Infrared Absorption Spectroscopy*, Holden Day, San Francisco, 1977.
57 L. M. Seaverson, S. Q. Luo, P. L. Chien and J. F. Mcclelland, *J. Am. Ceram. Soc.*, 1986, **69**, 243.
58 P. Apte, H. Burke and H. Pickup, *J. Mater. Res.*, 1992, **7**, 706.
59 V. Saraswati, G. V. N. Rao and G. V. Rama Rao, *J. Mater. Sci.*, 1987, **22**, 2529.
60 Ph. Colomban, *J. Mater. Sci.*, 1989, **24**, 3002.
61 JCPDS Powder Diffraction Data base, Joint Committee on Powder Diffraction Standards, International Center of Diffraction Data, Swarthmore, PA, 1990.
62 M. E. Smith, *Appl. Magn. Reson.*, 1993, **4**, 1.
63 W. Jung, S. Ahn and D. Kim, *J. Mater. Chem.*, 1998, **8**, 1869.
64 D. R. Mullins, S. H. Overbury and D. R. Huntley, *Surf. Sci.*, 1998, **409**, 307.
65 A. Pfau and K. D. Schierbaum, *Surf. Sci.*, 1994, **321**, 71.
66 H. Heikkinen, L. Johansson, E. Nykaenen and L. Niinisto, *Appl. Surf. Sci.*, 1998, **133**, 205.
67 E. Paparazzo, *Surf. Sci.*, 1990, **234**, L253.
68 Y. Zhou and M. N. Rahman, *Acta. Mater.*, 1997, **45**, 3635.
69 S. R. Rotman, R. P. Tandon and H. L. Tuller, *J. Appl. Phys.*, 1985, **57**, 1951.
70 Z. Qian and S. L. Shi, *Proc. 4th Int. Conf. Nanostr. Mater.*, 1998.
71 A. R. West, *Solid State Chemistry and its Applications*, Wiley, Chichester, New York, 1984.

Paper 9/03664D